Steel and Composite Structures, *Vol. 22, No. 6 (2016) 1359-1389*
DOI: http://dx.doi.org/10.12989/scs.2016.22.6.1359

Buckling and dynamic characteristics of a laminated cylindrical panel under non-uniform thermal load

Vinod S. Bhagat [a], Jeyaraj Pitchaimani [*] and S.M. Murigendrappa [b]

Department of Mechanical Engineering, National Institute of Technology Karnataka, Surathkal, Mangalore, 575025, India

(*Received July 15, 2016, Revised November 10, 2016, Accepted November 25, 2016*)

Abstract. Buckling and free vibration behavior of a laminated cylindrical panel exposed to non-uniform thermal load is addressed in the present study. The approach comprises of three portions, in the first portion, heat transfer analysis is carried out to compute the non-uniform temperature fields, whereas second portion consists of static analysis wherein stress fields due to thermal load is obtained, and the last portion consists of buckling and pre-stressed modal analyzes to capture the critical buckling temperature as well as first five natural frequencies and associated mode shapes. Finite element is used to perform the numerical investigation. The detailed parametric study is carried out to analyze the effect of nature of temperature variation across the panel, laminate sequence and structural boundary constraints on the buckling and free vibration behavior. The relation between the buckling temperature of the panel under uniform temperature field and non-uniform temperature field is established using magnification factor. Among four cases considered in this study for position of heat sources, highest magnification factor is observed at the forefront curved edge of the panel where heat source is placed. It is also observed that thermal buckling strength and buckling mode shapes are highly sensitive to nature of temperature field and the effect is significant for the above-mentioned temperature field. Furthermore, it is also observed that the panel with anti-symmetric laminate has better buckling strength. Free vibration frequencies and the associated mode shapes are significantly influenced by the non-uniform temperature variations.

Keywords: cylindrical panel; thermal buckling; non-uniform heating; finite element analysis; free vibration

1. Introduction

Laminated composite materials are gaining wider use in many engineering applications due to their higher stiffness and strength, and very low thermal coefficient in the fibre direction. Laminated cylindrical panel has been used in the components of supersonic and hypersonic aircrafts, nuclear reactors and highly inflammable fluid storage tanks. With the increased awareness of potential of laminated cylindrical panel, research on its failure mechanism have received considerable attention. Thin cylindrical panel like structures used in rockets, aircraft with

*Corresponding author, Assistant Professor, E-mail: jeyaraj@nitk.ac.in
[a] Research Scholar, E-mail: vinbha2011@gmail.com
[b] Associate Professor, E-mail: smm@nitk.ac.in

http://www.techno-press.org/?journal=scs&subpage=6 ISSN: 1229-9367 (Print), 1598-6233 (Online)

high-speed, and the spacecraft's, are exposed to extreme thermal load during their service, thus may subjected to thermal buckling and affects the dynamic characteristics due to the developed thermal pre-stress. Hence, buckling and dynamic characteristics of a laminated cylindrical panel exposed to thermal load is considered to be important factors in the design process.

Buckling strength of the cylindrical panel under uniform thermal load has been addressed in many of the literatures (e.g., Chen and Chen 1987, Chang and Chiu 1991, Thangaratnam *et al.* 1990). Gupta and Wang (1973) have employed Rayleigh-Ritz method to evaluate the buckling temperature of orthotropic cylindrical shells. Buckling behavior of simply supported and clamped uniformly heated cylindrical panels was analyzed by Chen and Chen (1987) using Galerkin's method. They found that buckling temperature was significantly influenced by the plate aspect ratio, fiber alignment, modulus ratio, boundary conditions and plate curvature. Thangaratnam *et al.* (1990) made use of finite element method to investigate the buckling behavior of laminated composite cylindrical and conical shells under thermal environment. They observed that the buckling behavior of laminated shell under thermal load is different from the mechanical load. Eslami and Javaheri (1999) investigated the buckling strength of the laminated composite cylindrical shells exposed to thermo-mechanical load.

Shen and Li (2002) examined the buckling and post-buckling of the shear deformable laminated cylindrical shells with geometric imperfections subjected to combined axial compression and uniform temperature loads. Patel *et al.* (2004) used finite element approach to analyze the buckling behavior of the cylindrical shells under thermal load. They incorporated higher-order theory based formulation which accounts for the transverse normal deformations and transverse shear. Critical buckling temperature of laminated composite shallow shells exposed to thermal loads was evaluated by Matsunaga (2007) by employing a two-dimensional global higher-order deformation theory. Patel *et al.* (2007) analyzed angle-ply laminated elliptical cylindrical shells exposed to the uniform thermal load. They studied the effects of the ply-angle and non-circularity on the critical buckling temperature and its corresponding mode shapes. First order shear deformation theory along with element-free kp-Ritz method was used by Zhao and Liew (2010) to observe the buckling behavior of functionally graded cylindrical shells subjected to thermal and mechanical load. State space approach was employed by Khdeir (2012) to obtain exact solutions for the thermoelastic behavior of cross-ply cylindrical, spherical and doubly curved shells exposed to arbitrary temperature field with different boundary conditions. Composite cylindrical shells reinforced by CNTs exposed to uniform temperature rise was investigated by Shen (2012). They employed higher order shear deformation theory to analyze the buckling and post buckling behavior. Topal (2013) maximized the thermal buckling strength of the laminated composite plates using extended layerwise approach. The first order shear deformation theory (FSDT) was employed to obtain the finite element solution and extended layerwise approach for optimization. Katariya and Panda (2016) employed higher order shear deformation theory to analyze the thermal buckling strength and vibration characteristics of uniformly heated laminated composite curved shell panel. Ahmadi and Pourshahsavari (2016) used differential quadrature method to analyze the buckling strength of functionally graded cylindrical panels. Rajanna *et al.* (2016) analyzed the laminated panels with and without cutouts to study the vibration and buckling behavior under compressive and tensile loads.

Kabir (1998) used first order shear deformation theory (FSDT) to study free vibration response of shear-flexible antisymmetric cross-ply laminated cylindrical panels. Mesh free kp-Ritz method was used by Zhao *et al.* (2004) to analyze the effects of different boundary conditions on the frequency behavior of the laminated cylindrical shells. Kurpa *et al.* (2010) made use of FSDT based R-function theory and variational methods to analyze the vibration behavior of laminated composite shells. Laminated cylindrical shells with thickness variations of linear, exponential, and sinusoidal was investigated by Viswanathan *et al*. (2011) to understand the free vibration behavior. They approximated the displacement function by using spline function techniques. Superposition-Galerkin Method (SGM) was employed by Mochida *et al*. (2012) to investigate the dynamic behavior of the double curved shallow shell. Yas *et al*. (2013) used the three-dimensional theory of elasticity to determine vibrational characteristics of functionally graded carbon nanotubes reinforced composite (FGCNTRC) cylindrical panels. They observed that the natural frequency of the shell is significantly influenced by kind of distribution and volume fraction of the CNT. Lei *et al*. (2013) analyzed the free vibration of FGCNTRC Cylindrical Panels by implementing the element-free kp- Ritz method. Micromechanical model based on the Eshelby-Mori-Tanaka approach was used to estimate the effective material properties. Topal (2012) optimized the frequency of the laminated composite plates using extended layerwise approach. The first order shear deformation theory (FSDT) was employed to obtain the finite element solution, whereas, extended layerwise approach for optimization. Zhang *et al*. (2014) analyzed carbon nanotube reinforced composite cylindrical panels for its flexural strength and free vibration by employing first order shear deformation theory. Mesh-free kp-Ritz method was used by Lei *et al*. (2014) to study the influence of static and periodic axial force on the dynamic stability of FGCNTRC cylindrical panels.

A few literatures (e.g., Ganapathi *et al*. 2002, Ganesan and Pradeep 2005, Jeyaraj 2013, Bhagat *et al*. 2016a) discussed on the free vibration behavior of cylindrical shells and plates subjected to thermal load. Ganapathi *et al*. (2002) studied thick laminated composite cylindrical shell under thermal/ mechanical load to examine its dynamic behavior using HSDT. Shell responses were obtained using finite element method in conjunction with the direct time integration technique. Circular cylindrical shells containing hot liquid was analyzed for its buckling and vibration behavior by Ganesan and Pradeep (2005) using semi-analytical finite element method. Initial stress effect and mass effect due to hot liquid was considered for the analysis. Pradyumna and Bandyopadhyay (2010) used higher-order shear deformation theory to investigate the free vibration and buckling behavior of singly and doubly curved functionally graded shell panels under thermal and uniaxial compressive load. Buckling and free vibration of isotopic plate exposed to non-uniform temperature field was examined by Jeyaraj (2013) using the finite element tool. Bhagat *et al*. (2016a) studied the buckling and the free vibration behavior of the isotropic cylindrical shell under thermal load using the finite element tool (ANSYS).

Based on the literature survey, in-depth analysis on combined buckling and free vibration behavior of laminated cylindrical panel under non-uniform thermal load has not been reported which is critical from the practical point of view. However, few literature reports on cylindrical shells under thermal environment were limited to either uniform or variation in, one-dimension or, in the thickness direction. In practice, because of un-symmetric geometric variation and the nature of heat source, most of the panels are exposed to arbitrarily varying non-uniform temperature fields. Structures used in aerospace vehicles such as high-speed aircraft, car panels located close to the engine, components of rockets and missiles, electronic circuit board, columns of heating furnace and nuclear vessels are typical examples of structures exposed to non-uniform heating during their service. Thin cylindrical shells under non-uniform temperature distribution are more susceptible to thermal buckling. As a whole, the non-uniform thermal load plays a vital role in determining and monitoring the structural design. Further, stresses developed due to non-uniform thermal load, significantly influences the free vibration behavior of the structures. The present study focuses on these aspects.

2. Analysis approach

Present study investigates the laminated cylindrical panel as shown in Fig. 1 subjected to non-uniform thermal load using a numerical approach to analyze the buckling and free vibration behavior. Fig. 2 shows the scheme of numerical approach followed in the present work. Numerical approach uses heat transfer analysis to get the non-uniform temperature field in accordance to thermal boundary constraint, then static analysis to compute the stress field under thermal load, and finally the buckling and pre-stressed modal analyzes to capture the critical buckling temperature as well as first five natural frequencies and associated mode shapes. A commercially available finite element tool ANSYS has been used to perform the numerical investigation.

2.1 Mathematical modelling

A cylindrical panel with thickness (h), length (L), width (W) and mean radius of curvature (R) investigated by finite element approach in the present study is as shown in Fig. 1. An orthogonal curvilinear coordinate system (x, y, z) is placed at the mid-surface of the panel. The rotations about the x- and y-directions are denoted as ϕ_x and ϕ_y respectively. Similarly, the in-plane displacements denoted by u, v and w are the functions of x-, y- and z-coordinates respectively. In heat transfer analysis, the cylindrical panel under uniform and non-uniform temperature field is modeled by using an eight noded isoparametric thermal shell element (shell 132), whereas, for static analysis panel has been modelled using an eight noded isoparametric structural shell element (shell 281). Initially, heat transfer analysis is performed to obtain the temperature distribution profile so that nodal temperatures are extracted and further these nodal values are then imported for static analysis to compute thermal stresses. These thermal stresses are used to perform eigenvalue buckling analysis to compute the critical buckling temperature of the panel. Finally, pre-stressed modal analysis is performed to obtain natural frequencies and associated mode shapes at a particular temperature. For the completeness, the finite element formulations for above all the cases considered are presented in the preceding sections (Khdeir 2012, Chang and Chiu 1991).

2.1.1 Heat transfer analysis

Temperature variation across the surface of the panel subjected to a particular type of heating is

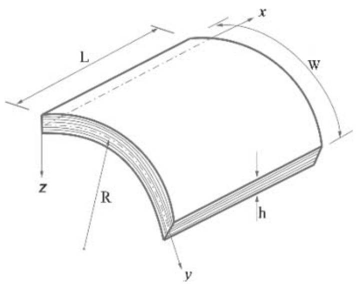

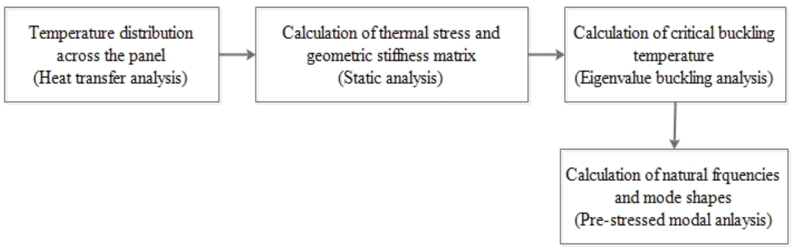

Fig. 1 Geometry of cylindrical panel

Fig. 2 A scheme of numerical analysis approach obtained by heat transfer analysis. For a two-dimensional differential equilibrium equation of system under steady-state heat conduction in the absence of heat generation is of the form

$$k_{xx}\frac{\partial^2 T}{\partial x^2}+k_{yy}\frac{\partial^2 T}{\partial y^2}=0 \tag{1}$$

where k_{xx} and k_{yy} are thermal conductivity in longitudinal and transverse direction, respectively, and T is the temperature. The variational form of the governing Eq. (1) is given by

$$I=\frac{1}{2}\int_a \{\Delta T\}^T[K_c]\{\Delta T\}da+\frac{1}{2}\int_{S_1} h_1 T^2 dS-\int_{S_1} h_1 T_\infty dS-\int_{S_2} qTdS \tag{2}$$

where h_1, ΔT, q, T_∞, S_1 and S_2 represent the convection heat transfer coefficient, temperature gradient vector, heat flux, ambient temperature, convection heat transfer boundary and heat flux specified boundary, respectively. Heat transfer in the panel is through conduction mode, thus, Eq. (2) reduces to

$$I=\frac{1}{2}\int\int \{\Delta T\}^T[K_c]\{\Delta T\}dxdy \tag{3}$$

By imposing the minimization condition to Eq. (3), yields

$$[K_c]\{T_e\}=\{0\} \tag{4}$$

where T_e is the nodal temperature vector and $[K_c]$ is the conduction matrix. With the help of Eq. (4), temperature distribution field on the cylindrical panel is obtained as per the temperature boundary constraints mentioned along the edges of the panel. To carry out the heat transfer analysis, thermal shell element (shell 132) is used. Subsequent to this, the structural analysis is carried out.

2.1.2 Structural analysis

The displacement fields u, v and w, at any point in a shell element are defined by Khdeir (2012)

$$\begin{aligned} u(x,y,z)&=u_0(x,y)+z\phi_x(x,y)\\ v(x,y,z)&=v_0(x,y)+z\phi_y(x,y)\\ w(x,y,z)&=w_0(x,y) \end{aligned} \tag{5}$$

where u_0, v_0 and w_0 are the mid-plane displacements and the linear strain-displacement relations at the mid-plane (z = 0 plane) are given by

$$\begin{Bmatrix} \varepsilon_{xx}\\ \varepsilon_{yy}\\ \gamma_{xy} \end{Bmatrix}=\{\varepsilon_0\}+z\{\kappa\} \tag{6a}$$

$$\begin{Bmatrix} \gamma_{yz} \\ \gamma_{xz} \end{Bmatrix} = \{\gamma_0\} \tag{6b}$$

where, $\{\varepsilon_0\}$, $\{\kappa\}$ and $\{\gamma_0\}$ are the linear strain vector, curvature vector and shear strains vector respectively given by

$$\varepsilon_0 = \begin{Bmatrix} \dfrac{\partial u_0}{\partial x} \\ \dfrac{\partial v_0}{\partial y} + \dfrac{w}{R} \\ \dfrac{\partial u_0}{\partial y} + \dfrac{\partial v_0}{\partial x} \end{Bmatrix} \tag{7a}$$

$$\kappa = \begin{Bmatrix} \dfrac{\partial \phi_x}{\partial x} \\ \dfrac{\partial \phi_y}{\partial y} \\ \dfrac{\partial \phi_x}{\partial y} + \dfrac{\partial \phi_y}{\partial x} \end{Bmatrix} \tag{7b}$$

$$\gamma_0 = \begin{Bmatrix} \phi_y + \dfrac{\partial w_0}{\partial y} - \dfrac{v}{R} \\ \phi_x + \dfrac{\partial w_0}{\partial x} \end{Bmatrix} \tag{7c}$$

The stress-strain relations for a laminated cylindrical panel considering thermal effects are as follows

$$\begin{Bmatrix} \sigma_{xx} \\ \sigma_{yy} \\ \tau_{xy} \\ \tau_{xz} \\ \tau_{yz} \end{Bmatrix} = \begin{bmatrix} Q_{11} & Q_{12} & 0 & 0 & 0 \\ Q_{21} & Q_{22} & 0 & 0 & 0 \\ 0 & 0 & Q_{66} & 0 & 0 \\ 0 & 0 & 0 & Q_{44} & 0 \\ 0 & 0 & 0 & 0 & Q_{55} \end{bmatrix} \begin{Bmatrix} \varepsilon_{xx} - \alpha_{xx}\Delta T(x,y) \\ \varepsilon_{yy} - \alpha_{yy}\Delta T(x,y) \\ \gamma_{xy} \\ \gamma_{yz} \\ \gamma_{xz} \end{Bmatrix} \tag{8}$$

where symbols used in the matrix are defined by

$$Q_{11} = \frac{E_{11}}{1-\upsilon_{12}\upsilon_{21}}; \quad Q_{22} = \frac{E_{22}}{1-\upsilon_{12}\upsilon_{21}}; \quad Q_{12} = \frac{\upsilon_{21}E_{11}}{1-\upsilon_{12}\upsilon_{21}}; \quad Q_{66} = G_{12}; \quad Q_{44} = G_{23}; \quad Q_{55} = G_{13}$$

$\Delta T(x,y)$ is the change in temperature with respect to a reference state (temperature variation along the panel surface). E_{11} and E_{22} are Young's moduli of laminated cylindrical panel in the principal material coordinates, α_{11} and α_{22} are coefficient of thermal expansion, υ_{12} and υ_{21} are Poisson's ratios and G_{12}, G_{13} and G_{23} are the shear moduli.

The relation between the stresses and strains obtained using first order shear deformation theory can be written as

$$\begin{Bmatrix} N \\ M \\ Qs \end{Bmatrix} = \begin{bmatrix} A & \overline{B} & 0 \\ \overline{B} & D & 0 \\ 0 & 0 & A^S \end{bmatrix} \begin{Bmatrix} \varepsilon_0 \\ \kappa \\ \gamma_0 \end{Bmatrix} - \begin{Bmatrix} N^T \\ M^T \\ 0 \end{Bmatrix} \tag{9}$$

Wherein in-plane stress resultant, moment resultant and transverse stress resultant, respectively defined as

$$N = \begin{Bmatrix} N_{xx} \\ N_{yy} \\ N_{xy} \end{Bmatrix} = \int_{-h/2}^{h/2} \begin{Bmatrix} \sigma_{xx} \\ \sigma_{yy} \\ \tau_{xy} \end{Bmatrix} dz \tag{10a}$$

$$M = \begin{Bmatrix} M_{xx} \\ M_{yy} \\ M_{xy} \end{Bmatrix} = \int_{-h/2}^{h/2} \begin{Bmatrix} \sigma_{xx} \\ \sigma_{yy} \\ \tau_{xy} \end{Bmatrix} zdz \tag{10b}$$

$$Qs = \begin{Bmatrix} Q_{xx} \\ Q_{yy} \end{Bmatrix} = \int_{-h/2}^{h/2} \begin{Bmatrix} \tau_{yz} \\ \tau_{xz} \end{Bmatrix} dz \tag{10c}$$

The thermal stress resultant N^T and thermal moment resultant M^T are given by

$$N^T = \int_{-h/2}^{h/2} [\alpha_{11} \;\; \alpha_{22} \;\; 0](Q_{11} + Q_{12})\Delta T(x,y)dz \tag{11a}$$

$$M^T = \int_{-h/2}^{h/2} [\alpha_{11} \;\; \alpha_{22} \;\; 0](Q_{11} + Q_{12})\Delta T(x,y)zdz \tag{11b}$$

The extensional A, coupling $\overline{B}$, bending D and transverse shear A^S,- stiffness are given by

$$\left(A_{ij} \;\; \overline{B}_{ij} \;\; D_{ij}\right) = \int_{-h/2}^{h/2} Q_{ij}\left(1 \;\; z \;\; z^2\right)dz \tag{12a}$$

$$\left(A_{ij}^S\right) = \chi \int_{-h/2}^{h/2} Q_{ij} dz \tag{12b}$$

where A_{ij}, $\overline{B}_{ij}$ and D_{ij} are defined for i, j =1, 2, 6 and i, j = 4, 5 in A_{ij}^S. χ denotes the shear correction factor.

Problem is evaluated by "*n*" numbers of shell element with eight nodes per element with each nodes of six degree-of-freedom. The displacement components, $\{U\}$ are approximated by the product of shape function matrix $[N_i]$ and nodal displacement vector $\{q_i\}$.

$$\{U\} = \sum_{i=1}^{8} [N_i]\{q_i\} \tag{13}$$

Shape functions for the 8-noded shell element are as follows

$$\begin{aligned}
N_1 &= \frac{1}{4}(1-\zeta)(1-\eta)(-\zeta-\eta-1) & N_5 &= \frac{1}{2}(1-\zeta^2)(1-\eta) \\
N_2 &= \frac{1}{4}(1-\zeta)(1-\eta)(\zeta-\eta-1) & N_6 &= \frac{1}{2}(1+\zeta)(1-\eta^2) \\
N_3 &= \frac{1}{4}(1+\zeta)(1+\eta)(\zeta+\eta-1) & N_7 &= \frac{1}{2}(1-\zeta^2)(1+\eta) \\
N_4 &= \frac{1}{4}(1-\zeta)(1+\eta)(-\zeta+\eta-1) & N_4 &= \frac{1}{2}(1-\zeta)(1-\eta^2)
\end{aligned} \tag{14}$$

By following the usual finite element procedure, structural stiffness matrix, geometric stiffness matrix and mass matrix can be obtained (Chang and Chiu 1991). The governing equation of the whole panel for static analysis is given by

$$[K]\{U\} = \{F\} \tag{15}$$

where $[K]$ is the structural stiffness matrix, $\{F\}$ is the thermal load vector and $\{U\}$ is the nodal displacement vector. The structural stiffness matrix and thermal load vector are given by

$$[K] = \iint [B]^T [C][B] dxdy \tag{16a}$$

$$\{F\} = \iint [B]^T \begin{bmatrix} N^T \\ M^T \end{bmatrix} dxdy \tag{16b}$$

where $[B]$ is the strain displacement matrix and $[C]$ is the constitutive matrix which states the stress-strain relation of the material. Similarly, the geometric stiffness matrix $[K_\sigma]$ determined from work done by the membrane forces developed due to thermal load and is given by

$$[K_\sigma] = \iint [G]^T \begin{bmatrix} N_{xx} & N_{xy} \\ N_{xy} & N_{yy} \end{bmatrix} [G] dxdy \tag{17}$$

where matrix $[G]$ is obtained from the derivatives of shape functions. Buckling analysis is performed by solving the following governing equation.

$$([K] + \lambda_i [K_\sigma])\{\psi_i\} = 0 \tag{18}$$

where λ_i is the eigenvalue and $\{\psi_i\}$ is the corresponding eigenvector for i^{th} buckling mode. The product of the temperature rise ΔT (above ambient temperature) and the lowest eigenvalue, λ_i gives the critical buckling temperature, T_{cr} (i.e., $T_{cr} = \lambda_1 \Delta T$).

In order to find the effect of thermal stress on the natural frequencies and its associated mode shapes, pre-stressed modal analysis is carried out by using Eq. (18).

$$\left(\left([K]+[K_\sigma]\right)-\omega_k^{2}[M]\right)\{\phi_k\}=0 \tag{19}$$

where, ω_k is the natural frequency of the pre-stressed structure, $\{\Phi_k\}$ the corresponding mode shape and $[M]$ is the structural mass matrix defined by

$$[M]=\iint [N]^T [\rho][N]dxdy \tag{20}$$

where $[N]$ is shape function matrix and $[\rho]$ is the inertia matrix.

3. Convergence and validation studies

3.1 Convergence study

Inorder to perform the convergence study, a laminated [0/90/90/0] cylindrical panel with CCCC boundary condition subjected to uniform thermal load is considered. Geometric parameters are thickness (h) = 0.001 m, width(W) = 0.1 m, length (L) = 0.1 m and radius of curvature ratio (R) = 0.5 m. Material properties; E_{11} = 181 GPa, E_{22} = 10.3 GPa, E_{33} = 10.3 GPa, $G_{12} = G_{13}$ = 7.17 GPa, G_{23} = 2.39 GPa, $v_{12} = v_{13} = v_{23}$ = 0.28, ρ = 1603 kg/m^3, α_1/α_2 = 0.02/22.5, k_1/k_2 = 4.62/0.72. Where E, G, v, α and K denote Young's modulus, Shear modulus, Poisson's ratio, coefficient of thermal expansion and thermal conductivity respectively, and the subscripts 1, 2, and 3 refer to the on-axis material coordinates. Variation of non-dimensional critical buckling temperature with different finite element mesh sizes is shown in Fig. 3. It is observed from Fig. 3 that, there is no change in buckling temperature for the mesh size beyond 20×20. Hence, cylindrical panel are analyzed with finite element mesh size of 20 × 20.

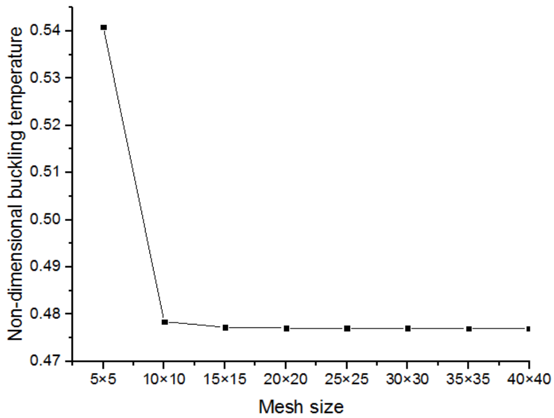

Fig. 3 Convergence study of [0/90/90/0] laminated cylindrical panel

3.2 Thermal buckling validation

The thermal buckling behavior of a composite layered $[15/\text{-}15]_3$ simply supported laminated cylindrical panel examined by Katariya and Panda (2016) under uniform temperature rise is considered for validation. The proportionate dimensions of the panel are $R/W = 5$ and $L/W = 1$ with following properties; $E_1/E_0 = 21$, $E_2/E_0 = 1.7$, $E_2/E_3 = 1$, $G_{12}/E_0 = 0.65$, $G_{23}/E_0 = 0.639$, $G_{12}/G_{13} = 1$, $v_{12} = v_{13} = v_{23} = 0.21$, $\alpha_1/\alpha_0 = -0.21$, $\alpha_2/\alpha_0 = \alpha_3/\alpha_0 = 16$, $\alpha_0 = 10^{-6}$/in/in/°F. Where E, G, v and α denote Young's modulus, Shear modulus, Poisson's ratio and coefficient of thermal expansion respectively, and the subscripts 1, 2, and 3 refer to the on-axis material coordinates. Katariya and Panda (2016) used higher order displacement functions based finite element method, while present method used FSDT. Critical buckling temperature predicted using the present method matches well with the results reported by Katariya and Panda (2016) as seen in Table 1.

3.3 Free vibration validation

A conical panel investigated by Jooybar *et al.* (2016) to analyze the free vibration behavior under thermal load has been considered for the validation. They obtained non-dimensional fundamental frequency of the conical panel using FSDT, while the present method uses FEA tool. The panel is made of ceramic (Si_3N_4) with the following mechanical and thermal properties; E = 348.43 GPa, $v = 0.24$ and $\rho = 2370$ kg/m^3, $k = 9.19$ W/mK, $\alpha = 5.8723 \times 10^{-6}$/K. The dimensions of the panel are $L/R_1 = 1$, $h/R_1 = 0.1$, $\beta = 60°$ and $\theta = 120°$. Non-dimensional natural frequency under thermal load obtained using present study shows good agreement with that of results reported in Jooybar *et al.* (2016) as shown in Fig. 4.

Table 1 Comparison of critical buckling temperature with Katariya and Panda (2016)

W/h	Non-dimensional critical buckling temperature		Difference in %
	Katariya and Panda (2016)	Present study	
40	0.854	0.877	2.6
100	0.547	0.568	3.8

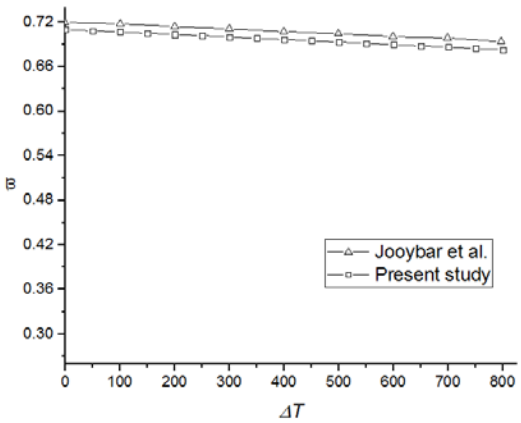

Fig. 4 Comparison of non-dimensional first natural frequency of conical panels under thermal load

4. Results and discussion

Buckling and dynamic characteristics of the cylindrical panel under thermal load is analyzed in the present study. Effect of different geometrical parameters on the buckling behavior of the panel exposed to different temperature variation fields is analyzed along with the boundary constraints. Similarly, the effect of different temperature variation fields on the free vibration behavior is also addressed. Throughout the analysis, a cylindrical panel with thickness (h) = 0.001 m, thickness ratio (W/h) = 100, aspect ratio (L/W) = 1 and curvature ratio (R/W) = 5 has been considered otherwise it is mentioned. Panel is assumed to be made of orthotropic material with following properties; E_{11} = 181 GPa, E_{22} = 10.3 GPa, E_{33} = 10.3 GPa, $G_{12} = G_{13}$ = 7.17 GPa, G_{23} = 2.39 GPa, $v_{12} = v_{13} = v_{23}$ = 0.28, ρ = 1603 kg/m^3, α_1/α_2 = 0.02/22.5, k_1/k_2 = 4.62/0.72, $\alpha_0 = 10^{-6}$/°C. Where E, G, v, α and K denote Young's modulus, Shear modulus, Poisson's ratio, coefficient of thermal expansion and thermal conductivity respectively, and the subscripts 1, 2, and 3 refer to the on-axis material coordinates. Present study focusses on the buckling and free vibration behavior of the cylindrical panel with two different laminate schemes, namely panel-1 with the lamination scheme of [0/90/90/0] and panel-2 with the lamination scheme of [0/90/0/90]. Five different in-plane temperature variation fields and four different structural boundary constraints CCCC, SSCC, SSSS and CCFC (where C- clamped, S-simply supported and F-free) has been considered. Table 2 shows that the first letter in these boundary constraints is associated with forefront curved edge at x = 0 in order. CCCC boundary constraints are applied to model the panel restrained from all sides. Further, SSSS boundary constraints are also used to evaluate the effect of relaxed constraints. Whereas, combined effect of simply supported and clamped panel is studied using SSCC boundary constraints. Finally, the effect of free edge on the buckling behaviour of the panel is investigated using CCFC boundary constraints. It is assumed that the material properties of the panel investigated are temperature independent. However, it is ensured that the temperature range analyzed does not change the material properties significantly with temperature rise.

4.1 Non-uniform temperature distributions

Present study deals with four different non-uniformly varying in-plane temperature distribution fields according to the nature of the assumed temperature source on a cylindrical panel. The uniform temperature field has also been considered for investigation, so that the change in buckling and free vibration behaviour of cylindrical panel with change in temperature field from uniform to non-uniform can be found. In the present analysis five cases of temperature variations are considered; case(i)-uniform temperature field; case(ii)-decreasing trend in temperature field; case(iii)- decreasing and increasing trend in temperature field; case(iv)-increasing and decreasing trend in temperature field and case(v)-Camel hump trend in temperature field (Bhagat *et al*. 2016b). Table 3 shows a cylindrical panel with the position of the heat source, associated temperature fields and thermal boundary constraints.

4.2 Studies on cylindrical panel under thermal load

Present study has been grouped into two parts. First part focuses on the effect of in-plane temperature variation and the geometric parameters on the thermal buckling and free vibration behaviour of the symmetric cross ply laminated cylindrical panel named as panel-1. Whereas the second part deals with the analysis of un-symmetric cross ply laminated cylindrical panel called as

Table 2 Different structural boundary constraints investigated

Structural boundary constraints							
CCCC		SSCC		SSSS		CCFC	
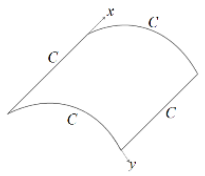		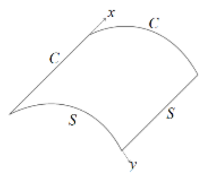		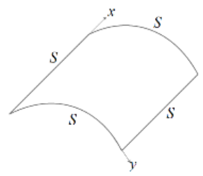		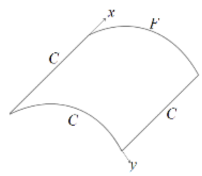	
$y = 0, W$	$u = v = w = 0$ $\theta_x = \theta_y = 0$	$y = W$ $y = 0$	$v = w = 0$ $\theta_x = 0$ $u = v = w = 0$ $\theta_x = \theta_y = 0$	$y = 0, W$	$v = w = 0$ $\theta_x = 0$	$y = 0, W$	$u = v = w = 0$ $\theta_x = \theta_y = 0$
$x = 0, L$	$u = v = w = 0$ $\theta_x = \theta_y = 0$	$x = 0$ $x = L$	$u = w = 0$ $\theta_y = 0$ $u = v = w = 0$ $\theta_x = \theta_y = 0$	$x = 0, L$	$u = w = 0$ $\theta_y = 0$	$x = 0$	$u = v = w = 0$ $\theta_x = \theta_y = 0$

Table 3 Different temperature distribution field analyzed

	Temperature distribution cases				
	Case(i)	Case(ii)	Case(iii)	Case(iv)	Case(v)
Position of heat source	Uniform	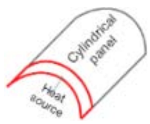	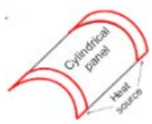	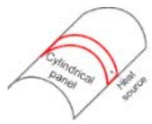	
Thermal distribution	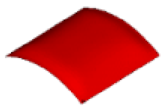		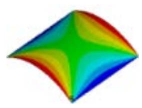	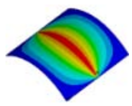	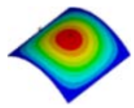
Boundary constraints	$T(x, y) = 1°C$	$T = 0°C$ at $y = 0; y = W$	$T = 0°C$ at $y = 0; y = W$	$T = 0°C$ at $y = 0; y = W$ $x = 0; x = L$	$T(x, y) = \sin(\pi x/W) \sin(\pi y/L)$
		$T = 1°C$ at $x = 0$ $T = 0°C$ at $x = L$	$T = 1°C$ at $x = 0; x = L$	$T = 1°C$ at $x = L/2$	

*Blue: ambient temperature; Red: 1°C above ambient temperature and others in-between

panel-2. Non-dimensional critical buckling temperature is given in Eq. (20). (Katariya and Panda 2016)

$$T_{cr}^{*} = \alpha_0 \times T_{cr} \times 10^3 \tag{21}$$

4.2.1 Studies on cylindrical panel-1

Thermal buckling studies

Buckling strength of a symmetric cross ply laminated cylindrical panel exposed to non-uniform heating is presented here. Effect of thickness ratio, aspect ratio, curvature ratio and structural boundary constraints on critical buckling temperature and associated mode shape are investigated in detail. In-order to obtain critical buckling temperature of the panel under non-uniform temperature field variations in terms of uniformly heated panels, critical buckling temperature, "Magnification factor of the first kind, η" given by Ko (2004) is used in the present study. The relation is

$$\eta = \frac{[T_o]_{cr}}{[T_c]_{cr}} \tag{22}$$

where $[T_o]_{cr}$ is the buckling temperature of a panel with non-uniform temperature field and $[T_o]_{cr}$ is critical buckling temperature of the panel under uniform temperature field. With this relation, critical buckling temperature of the panel-1 under uniform temperature field is used to obtain the buckling temperature of the panel-1 under non-uniform temperature field. In this analysis, a temperature of 1°C above ambient is considered as a peak temperature (T_o) whereas the heat sink temperature (T_s) is varied in the range of (T_s/T_o = 0 to 1), which is then used to establish the relation for different temperature cases. Magnification factor of first kind for different non-uniform temperature fields is shown in Table 4, for CCCC panel-1. $T_s/T_o = 0$ in Table 4 shows that, the panel-1 is subjected to a peak temperature of 1°C above ambient while heat sink is maintained at ambient temperature, which in other words, states that panel-1 is subjected to non-uniform temperature field with a higher temperature difference. Panel-1 with both heat-sink and peak temperature at 1^{o}C above ambient is indicated by $T_s/T_o = 1$ which means that panel-1 is subjected to uniform temperature distribution field. From the values indicated by η, it can be clearly seen that nature of temperature variation has a high impact on the thermal buckling strength of the panel-1. Table 4 reveals that the critical buckling temperature of a panel-1 under case(ii) temperature field can be obtained by magnifying the case(i) temperature field with a factor of 3.10. Similarly, critical buckling temperature of a panel-1 under case(iii), case(iv) and case(v) temperature fields can be obtained by a magnifying factor of 1.56, 2.21, 1.72 respectively. Table 4 also shows that among all non-uniform temperature field, case(iii) has the lowest buckling temperature as in case(iii) temperature field, the maximum temperature variation is observed at the major portion of the panel-1. It is also noted that case(v) has relatively less buckling strength compared to case(ii) and case(iv). From the above observation, it can be concluded that the thermal stress developed will be more when the major portion of the panel-1 surface is exposed to higher temperature and the resulting membrane force reduces the buckling strength of the panel-1.

Table 4 Non-dimensional critical buckling temperature and magnification factor of first kind for CCCC cylindrical panel-1

T_s/T_o	Case(ii)		Case(iii)		Case(iv)		Case(v)	
	T^*_{cr}	η	T^*_{cr}	η	T^*_{cr}	η	T^*_{cr}	η
0.0	1.47	3.10	0.74	1.56	1.05	2.21	0.82	1.72
0.2	1.04	2.19	0.67	1.44	0.85	1.78	0.72	1.51
0.4	0.80	1.68	0.60	1.25	0.71	1.49	0.63	1.34
0.6	0.65	1.37	0.55	1.19	0.61	1.28	0.57	1.20
0.8	0.55	1.15	0.51	1.06	0.53	1.12	0.52	1.09
1.0*	0.47	1.00	0.47	1.00	0.47	1.00	0.47	1.00

*Case(i) temperature field

Table 5 Non-dimensional critical buckling temperature and magnification factor of first kind for CCFC cylindrical panel-1

T_s/T_o	Case(ii)		Case(iii)		Case(iv)		Case(v)	
	T^*_{cr}	η	T^*_{cr}	η	T^*_{cr}	η	T^*_{cr}	η
0	3.68	2.09	3.09	1.75	3.43	1.95	3.32	1.89
0.2	3.05	1.73	2.70	1.53	3.21	1.83	3.18	1.81
0.4	2.59	1.47	2.39	1.36	2.87	1.63	2.77	1.57
0.6	2.24	1.27	2.14	1.22	2.42	1.37	2.33	1.33
0.8	1.97	1.12	1.93	1.10	2.04	1.16	2.01	1.14
1.0*	1.76	1.00	1.76	1.00	1.76	1.00	1.76	1.00

*Case(i) temperature field

As the panels with free edge behaves differently from the all edges clamped panel under thermal load, a CCFC cylindrical panel-1 is analyzed. Table 5 depicts the magnification factor of first kind for CCFC panel-1. It is clear from Table 5 that buckling strength of panel-1 is influenced by the nature of temperature variation irrespective of its edge conditions. However, the buckling behavior of the CCFC panel-1 with the nature of temperature variation is not similar to the CCCC panel-1. Unlike the CCCC panel-1, temperature at the free edge for a given temperature variation determines the buckling strength of CCFC panel-1. From Table 5 it is found that, the buckling temperature for case(ii), case(iii), case(iv) and case(v) temperature field can be obtained by magnifying the buckling temperature under case(i) with a factor of 2.09, 1.75, 1.95 and 1.89 respectively. It can be clearly seen from Tables 4-5 that CCCC cylindrical panel-1 has poor buckling strength compared to the CCFC panel-1. It is anticipated, as CCFC boundary constraint, panel-1 is allowed to expand freely along the direction of free edge, thus amount of stress developed in CCFC panel-1 is less than the CCCC panel-1. However, membrane forces developed due to thermal stress is less in CCFC panel-1 making it to buckle at higher temperature.

The effect of thickness ratio on the buckling strength of the panel-1 subjected to different temperature variation fields is shown in Figs. 5(a)-(b) respectively, for CCCC and CCFC edge conditions. It is clearly seen from Fig. 5 that buckling temperature decreases with increase in

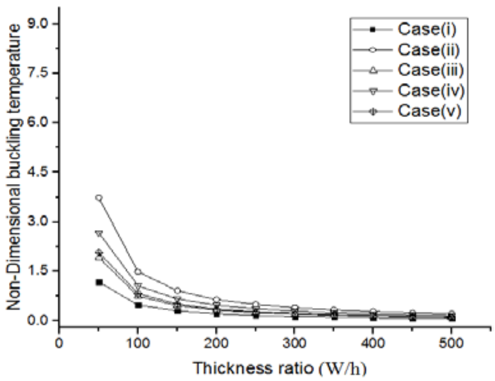

(a) CCCC

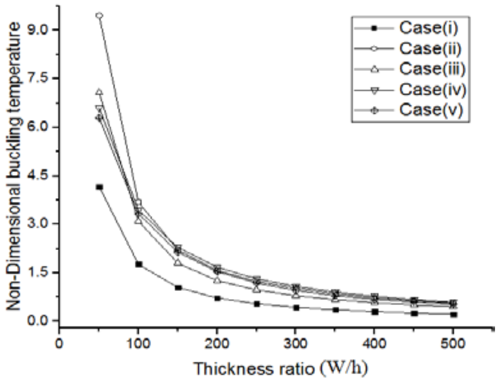

(b) CCFC

Fig. 5 Influence of thickness ratio and temperature variation on buckling strength of cylindrical panel-1

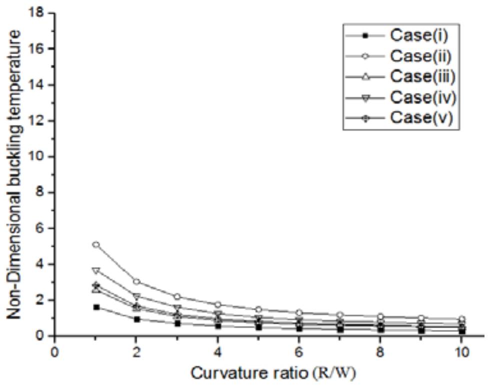

(a) CCCC

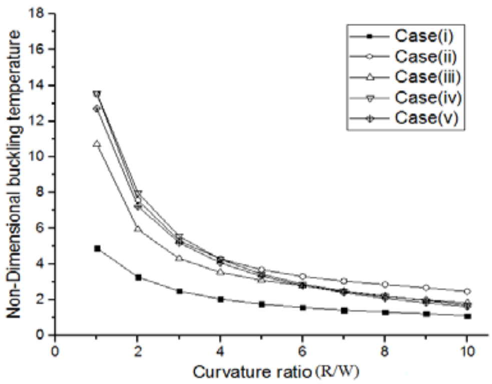

(b) CCFC

Fig. 6 Influence of curvature ratio and temperature variation on buckling strength of cylindrical panel-1

thickness ratio. This behavior of the panel-1 indicates that the stiffness of the panel-1 decreases with the increase in thickness ratio making it to buckle at low temperature. It can be well observed from Figs. 5(a)-(b) that the variation in the buckling strength of panel-1 for different temperature cases is significantly influenced by the thickness ratio at lower values whereas the variation is minimal at higher values of thickness ratio. At higher values of thickness ratio, the width of the cylindrical panel-1 is found to be more which increases the non-supporting area of the panel-1 thus making it very less stiff. And at this stiffness, small membrane forces are sufficient to cause thermal buckling. It is also noted that, the CCFC panel-1 always has better buckling strength compared to CCCC panel-1 due to free edge associated with it. From Figs. 5(a)-(b), it is also observed that, panels exposed to case (i) temperature field has a poor buckling strength while case(ii) temperature field results in better buckling strength it is due to amount of membrane forces generated by thermal load is more in case(i) temperature field compared to case(ii) temperature field.

An effort has been made to study the effect of amount of curvature on the buckling strength of the cylindrical panel-1 when subjected to different temperature profile. Figs. 6(a)-(b) shows the influence of curvature ratio on the buckling temperature of the panel-1 under CCCC and CCFC boundary constraints. Influence of curvature ratio on the buckling temperature of the panel-1 is similar to that of thickness ratio wherein buckling temperature decreases with the increase in curvature ratio. This behavior of the panel-1 is mainly due to change in moment of inertia with the curvature ratio. With the increase in curvature ratio the moment of inertia decreases, which inturn decreases the bending stiffness of the panel-1 and thus lowers the buckling strength of the panel-1. At a lower curvature ratio, variation in the buckling temperature for different temperature cases is quite noticeable. Under case(ii) temperature field location of heat source was found to be close to the fixed support and the membrane forces developed due to temperature variation is well poised by support reaction forces. Thus panel-1 under case(ii) requires more amount of heat to develop sufficient membrane force that causes buckling. Since the heat source is located away from the fixed support where the panel-1 is less stiff, case(iv) and case(v) was observed to have less buckling strength than the panel-1 with case(ii) temperature field. Along with the location of the heat source, the amount of heat supplied plays an important role in determining the buckling strength of the panel-1. Panel-1 under case(iii) temperature field has a heating source at the fixed supports where it is more stiff, but still produces high membrane forces due to amount of heat given is more in case(iii) temperature field compared to case(ii), case(iv) and case(v) temperature fields. Furthermore, panel-1 under case(i) is fully exposed to uniform heat, making it to buckle at a lower temperature compared to all other temperature fields.

Figs. 7(a)-(b) shows the effect of aspect ratio on the buckling temperature of the panel-1 under different temperature variation fields. It is interesting to know that the panel-1 behaves differently under different temperature fields with the change in aspect ratio. It can be noted from Fig. 7(a), that as the aspect ratio increases buckling strength of the CCCC panel-1 under case(i) and case(v) temperature fields decreases whereas for other temperature fields buckling strength increases. Stiffness of the panel-1 decreases with the increase in aspect ratio, thus the amount of heat applied and its location decides the buckling strength of the panel-1 under different aspect ratio. Under case(i) temperature field, the CCCC panel-1 is fully exposed to the peak temperature, making it to buckle at lower temperature with the increase in aspect ratio. Similarly, for the CCCC panel-1 under case(v) temperature field, the heat is applied at the less stiff area which increases with the aspect ratio thus buckles at lower temperature. However, for other temperature fields membrane forces generated due to heat, decreases with the increase in aspect ratio, which thus increases the buckling strength of the panel-1. Unlike CCCC panel-1, CCFC panel-1 under case(ii), case(iii) and case(iv) behaves similar to the case(i) and case(v) temperature fields as shown in Fig. 7(b). Wherein buckling strength of the CCFC panel-1 decreases with the aspect ratio of the panel-1

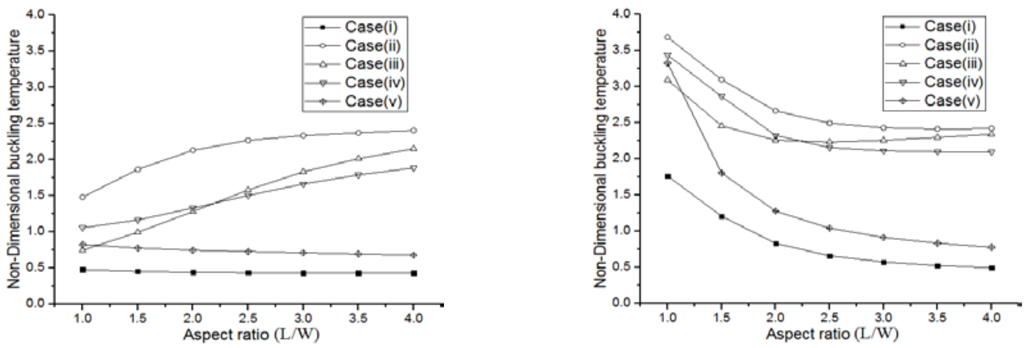

(a) CCCC (b) CCFC

Fig. 7 Influence of aspect ratio and temperature variation on buckling strength of cylindrical panel-1

Table 6 Effect of thickness ratio on the buckling mode shape of CCCC panel-1

W/*h*	Case(i)	Case(ii)	Case(iii)	Case(iv)	Case(v)
100	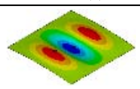	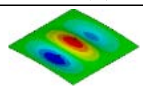	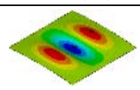	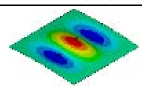	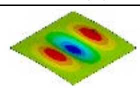
200	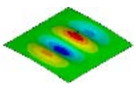	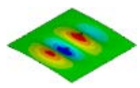	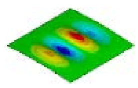	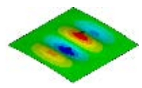	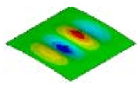
300	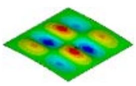	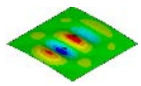	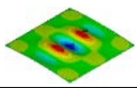	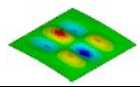	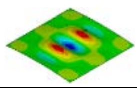

*Note: Color gradients followed with dark-red and dark-blue indicate peak and trough buckling displacements, respectively

Table 7 Effect of thickness ratio on the buckling mode shape of CCFC panel-1

W/h	Case(i)	Case(ii)	Case(iii)	Case(iv)	Case(v)
100	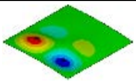	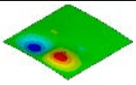	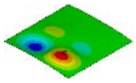	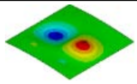	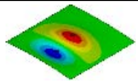
200	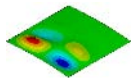	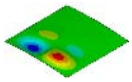	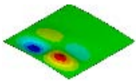	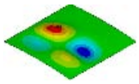	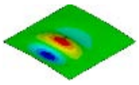
300	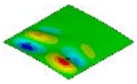	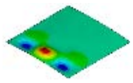	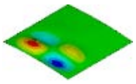	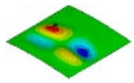	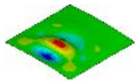

*Note: Color gradients followed with dark-red and dark-blue indicate peak and trough buckling displacements, respectively.

under all temperature fields. Along with the aspect ratio, the free edge of the CCFC panel-1 adds in lowering the stiffness of the panel-1 which thus decreases the buckling strength of the panel-1.

Influence of thickness ratio and non-uniform temperature field on fundamental buckling mode shape of the CCCC panel-1 and CCFC panel-1 are given in Tables 6 and 7, respectively. From Table 6, it is clear that the buckling mode shape of the CCCC panel-1 is highly influenced by the thickness ratio, while it is not much influenced by the nature of non-uniform heating. Change in buckling mode shape with increase in thickness ratio can be attributed to decrease in structural stiffness with increase in thickness ratio. Table 6 also reveals that the CCCC- panel 1 under case(ii) temperature field was observed to have maximum bending amplitude in the area exposed to peak temperature and the area opposite to it experiences least bending amplitude. For the CCCC panel-1 subjected to case(ii), case(iii) and case(v) temperature fields, buckling mode shapes observed does not change significantly with the thickness ratio but their modal indices along longitudinal direction increases with the thickness ratio. Further for the CCCC panel-1 under case(i) and case(iv) temperature fields, at higher value of thickness ratio, modal indices of the buckling mode shapes along with longitudinal direction changes in circumferential direction too. From Table 7, it is clear that, buckling mode shapes and its indices observed under CCFC panel-1 is totally different from that of CCCC panel-1. Buckling mode shape of the CCFC panel-1 is influenced by both the thickness ratio and the nature of temperature variation. CCFC panel-1 under case(iv) and case(v) temperature fields has a heat source at the central location where the structural stiffness is minimum. Thus the buckling mode shape with maximum bending amplitude is found to be at a central location. Whereas for all other temperature cases the maximum bending amplitude of buckling mode shape was found to be at location away from the free edge.

Influence of temperature variation and curvature ratio on the buckling mode shape is shown in Tables 8-9 for CCCC and CCFC panel-1 respectively. It is known that the moment of inertia changes with the curvature ratio and its effect can be seen on the buckling mode shape and its modal indices. Table 8 reveals that the buckling modal indices for a given temperature field is highly influenced by the curvature ratio of the CCCC panel-1. It is also observed that at higher curvature ratio, there is not much variation in the bending amplitude and the modal indices of the CCCC panel-1 for different temperature fields. However, variation of buckling mode shape of CCFC panel-1 with curvature ratio and non-uniform temperature field is different compared to the CCCC panel-1 as seen in Table 9. Table 9 also clearly indicates that nodal and anti-nodal lines of a buckling mode occurs where the highest temperature of a particular temperature field occurs. It

Table 8 Effect of curvature ratio on the buckling mode shape of CCCC panel-1

R/*W*	Case(i)	Case(ii)	Case(iii)	Case(iv)	Case(v)
1	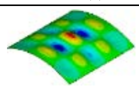	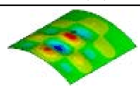	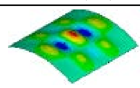	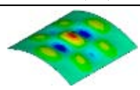	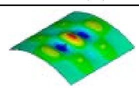
5	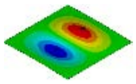	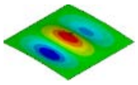	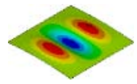	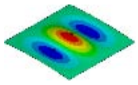	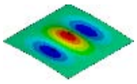
10	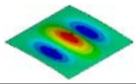	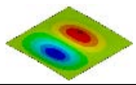	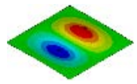	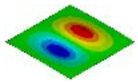	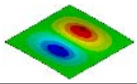

*Note: Color gradients followed with dark-red and dark-blue indicate peak and trough buckling displacements, respectively.

Table 9 Effect of curvature ratio on the buckling mode shape of CCFC panel-1

R/*W*	Case(i)	Case(ii)	Case(iii)	Case(iv)	Case(v)
1	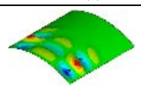	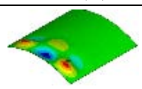	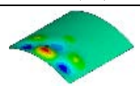	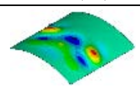	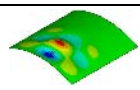
5	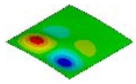	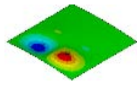	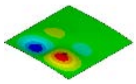	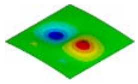	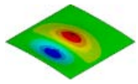
10	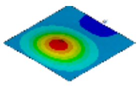	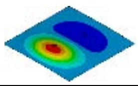	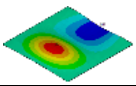	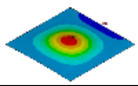	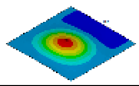

*Note: Color gradients followed with dark-red and dark-blue indicate peak and trough buckling displacements, respectively.

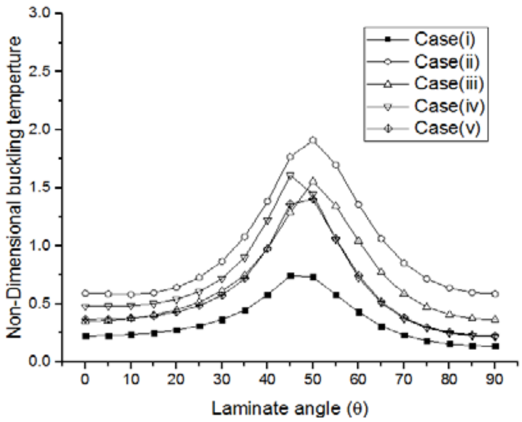

Fig. 8 Effect of laminate orientation on buckling strength of CCCC panel-1

can be clearly seen for higher curvature ratio cases. Study also shows that modal indices of the buckling modes decreases with the increase in curvature ratio along the longitudinal and transverse direction.

In order to study the effect of laminate orientation on the buckling temperature of CCCC panel-

1, an analysis is carried on a symmetric angle ply laminate having an orientation of [θ/-θ/-θ/θ]. Fig. 8 reveals that the buckling temperature of the panel-1 is significantly influenced by the laminate orientation of symmetric angle ply. This can be attributed to change in stiffness of the panel-1 due to change in elastic constants and thermal coefficient with the laminate orientation. It can be noted that buckling temperature of the panel-1 increases with the laminate orientation and attains the maximum value at 45°~50° and it then reduces with further increase in laminate angle. Similarly, CCCC panel-1 exposed to case(ii) temperature field has a better thermal buckling strength while case(i) temperature field results in poor buckling strength. Fig. 8 suggests that fiber angle can be effectively used to control the thermal buckling strength of the laminated composite panel-1.

Structural boundary constraints of the panel are considered as the highly influencing factor in developing thermal stress. And to visualize it, a study has been carried out on the panel-1 with four different structural boundary constraints and results are shown in Table 10. It can be seen that CCCC panel-1 has the lowest buckling strength compared to others. Panel-1 under CCCC boundary provide constraints from all sides, thus does not allow any free expansion which leads to development of high thermal stresses. Whereas CCFC panel-1 allows free expansion from one of its side due to free edge and because of which CCFC panel-1 buckles at a higher temperature than CCCC panel-1. Panel-1 under SSSS boundary constraints was observed to have highest buckling strength. SSSS boundary constraints of the panel-1 doesn't allow any in-plane motion, but allows rotation, which makes panel-1 to relive some stress through rotation thus produces less membrane forces. Panel-1 with case(i) temperature field has the minimum buckling strength under all boundary constraints. Similarly, panel-1 under case(ii) temperature field has the lowest buckling temperature. It is also noted that panel-1 under case(iv) temperature field has the highest buckling temperature than the case(iii) under CCCC, SSCC and CCFC boundary constraints due to amount of heat supplied to the panel-1 under case(iv) is less than the case(iii) temperature field. Whereas panel-1 under SSSS boundary constraints, case(iii) has the highest strength than case(iv) and this

Table 10 Effect of boundary constraints on the non-dimensional buckling temperature of panel-1

Boundary constraints	Temperature field				
	Case (i)	Case (ii)	Case (iii)	Case (iv)	Case (v)
CCCC	0.47	1.48	0.74	1.05	0.82
SSCC	1.43	5.37	2.58	2.87	2.55
SSSS	3.27	6.31	5.90	4.59	4.35
CCFC	1.76	3.68	3.093	3.43	3.32

Table 11 Effect of lamination scheme and temperature fields on the non-dimensional buckling temperature of CCCC panel-1

Lamination scheme	Case (i)	Case (ii)	Case (iii)	Case (iv)	Case (v)
0/90/90/0	0.47	1.47	0.74	1.05	0.82
0/90/0/90	0.69	1.99	1.10	1.68	1.23
45/-45/-45/45	0.74	1.76	1.28	1.61	1.36
45/-45/45/-45	0.92	2.17	1.55	2.28	1.78
0/45/-45/90	0.61	1.35	0.86	1.57	1.14

Table 12 Effect of lamination scheme and temperature fields on the non-dimensional buckling temperature of CCFC panel-1

Lamination scheme	Case (i)	Case (ii)	Case (iii)	Case (iv)	Case (v)
0/90/90/0	1.76	3.68	3.09	3.43	3.32
0/90/0/90	1.48	3.07	1.72	3.64	3.37
45/-45/-45/45	0.84	1.77	1.50	1.79	1.55
45/-45/45/-45	1.08	2.20	1.83	2.52	2.06
0/45/-45/90	0.94	1.55	1.22	2.02	1.52

can be attributed to the amount of stress generated mainly due to non-uniform temperature variation is more in case(iv) than in case(iii) temperature field. Panel-1 under SSCC boundary constraints follows combined trend of CCCC and SSSS boundary constraints, thus buckling temperature recorded for SSCC panel-1 lies between the CCCC and SSSS panel-1.

Free vibration analysis

In order to study the influence of thermal effect on the behavioral trend of free vibration and its mode shape, a pre-stressed modal analysis has been carried out on a cylindrical panel-1 exposed to five different temperature variation fields. Cylindrical panel-1 with a lamination scheme [0/90/90/0] is considered for the detailed investigation and the results are given in Table 13. Table 13 presents the influence of thermal load on the natural frequencies of the panel. To demonstrate, thermal loads with 50 and 95% of the critical buckling temperature, T_{cr} have been considered. Irrespective of structural boundary constraints and nature of temperature fields, the natural frequencies reduce with increase in temperature, as observed by (Ganesan and Pradeep 2005, Jeyaraj 2013). This happens due to reduction in structural stiffness with increase in thermal stress, which is independent of edge conditions. In a design of thin structural cylindrical panels, along with the free vibration frequency, mode shape also plays a vital role as it determines the nodal and anti-nodal position of the particular mode through which mode can be excited. Hence it is very important to know the effect of thermal load on the mode shape variation along with the frequency.

Table 13 Effect of thermal load on free vibration frequency (Hz) of panel-1

Boundary constraint	Mode	At ambient temp.	Case(i)		Case(ii)		Case(iii)		Case(iv)		Case(v)	
			Critical buckling temperature, T_{cr} in %									
			50%	95%	50%	95%	50%	95%	50%	95%	50%	95%
CCCC	1	2325	2067	789	2077	785	2076	784	2082	779	2072	795
	2	2664	2119	1096	2139	1154	2135	1117	2091	1138	2107	1050
	3	2876	2510	1978	2522	2002	2512	2011	2545	1975	2533	1978
	4	3304	2667	2151	2713	2190	2726	2140	2603	2105	2677	2233
CCFC	1	2260	2110	882	2157	930	2058	928	2031	759	1980	746
	2	2354	2138	1728	2236	1537	2128	1055	2211	1576	2049	1094
	3	2705	2352	1925	2373	2041	2178	1627	2226	1888	2271	1669
	4	2771	2386	1952	2541	2219	2366	1803	2403	2216	2358	1797

Table 14 Effect of thermal load on the free vibration mode shape of panel-1

	Mode	CCCC				CCFC			
		1	2	3	4	1	2	3	4
Temp. Variation	At Ambient Temp.								
Case(i)	50%T_{cr}								
	95%T_{cr}								
Case(ii)	50%T_{cr}								
	95%T_{cr}								
Case(iii)	50%T_{cr}								
	95%T_{cr}								
Case(iv)	50%T_{cr}								
	95%T_{cr}								
Case(v)	50%T_{cr}								
	95%T_{cr}								

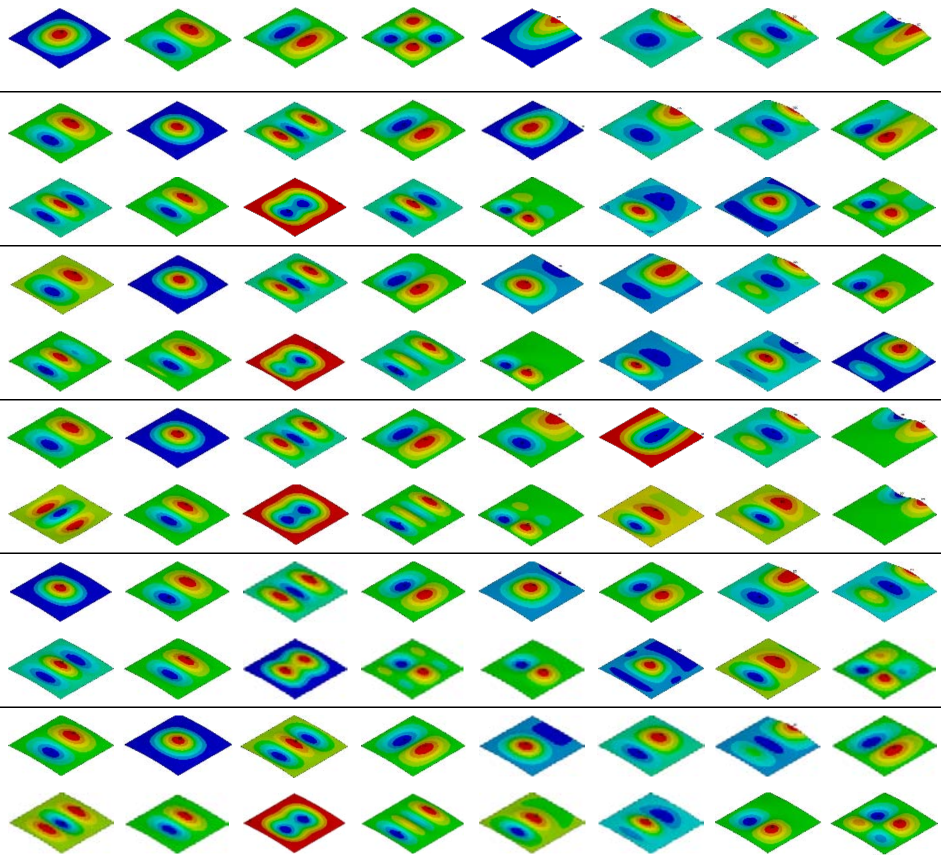

Variation in free vibration mode shapes of the panel-1 with the increase in temperature is shown in Table 14. It is found that, the free vibration mode shapes are significantly influenced by the rise in temperature under all the temperature fields considered in the present study. Shifting of modes and moving of nodal and anti-nodal positions are commonly observed for the panel-1 under different temperature fields. For example, mode 1 of CCCC panel-1 having modal indices of (1,1) at ambient temperature changes to (1,3) at 95% of the critical buckling temperature under case(i), case(ii), case(iv) and case(v) temperature field whereas it changes to (3,1) for case(iii) temperature field as seen in Table 14. It is also observed that for the CCFC panel-1, with increase in temperature, anti-nodal position of modes is moving towards the fixed edge. For example, under case(i), case(ii) and case(iii) temperature field, free vibration modes at ambient temperature under mode 1 is found to occur at the free edge but it shifts towards the fixed edge with the increase in temperature. This is due to the fact that; panel-1 becomes soft at the free edge with the increases in temperature, thus making the vibration modes to shift towards the stiffer side of the panel-1. From Table 14 it is also revealed that free vibration mode shapes of the panel exposed to a temperature near the critical buckling temperature are similar to its buckling mode shape.

4.2.2 Studies on cylindrical panel 2

To analyze the effect of un-symmetric cross ply on the buckling and free vibration behavior of a panel exposed to different temperature variation fields, cylindrical panel-2 is considered. It is assumed that panel-2 has same geometric parameters of panel-1 except the lamination scheme.

Thermal buckling studies

Different investigations are carried out on panel-2 also to analyze the influence of different parameters on thermal buckling strength and free vibration behavior. Magnification factor of the first kind obtained for CCCC panel-2 is shown in Table 15. It can be seen from Tables 4 and 16 that the variation in the magnification factor of a CCCC panel-2 is similar to CCCC panel-1. The buckling temperature of CCCC panel-2 under case(i) temperature field has to be magnified by 2.87, 1.58, 2.42 and 1.78 to obtain the buckling temperature of case(ii), case(iii), case(iv) and case(v) temperature field respectively. It is found from Table 15 that CCCC panel-2 under case(ii) temperature field has the highest buckling temperature compared to other temperature fields. It is mainly due to, heat applied under case(ii) temperature field is at the clamped edge of the CCCC panel-2 and the membrane forces generated at that edge balances with the reaction forces and less membrane forces are found to be act on the panel-2 under case(ii) temperature field thus high magnification factor is observed. Table 15 also shows that, irrespective of the lamination scheme,

Table 15 Non-dimensional critical buckling temperature and magnification factor of first kind for CCCC cylindrical panel-2

T_s/T_o	Case(ii)		Case(iii)		Case(iv)		Case(v)	
	T^*_{cr}	η	T^*_{cr}	η	T^*_{cr}	η	T^*_{cr}	η
0.0	1.99	2.87	1.10	1.58	1.68	2.42	1.23	1.78
0.2	1.49	2.14	0.99	1.43	1.33	1.92	1.08	1.56
0.4	1.17	1.69	0.91	1.31	1.10	1.59	0.96	1.39
0.6	0.96	1.38	0.82	1.19	0.93	1.33	0.87	1.25
0.8	0.80	1.16	0.75	1.08	0.79	1.14	0.77	1.11
1.0*	0.69	1.00	0.69	1.00	0.69	1.00	0.69	1.00

*Case(i) temperature field

Table 16 Non-dimensional critical buckling temperature and magnification factor of first kind for CCFC cylindrical panel-2

T_s/T_o	Case (ii)		Case(iii)		Case(iv)		Case(v)	
	T^*_{cr}	η	T^*_{cr}	η	T^*_{cr}	η	T^*_{cr}	η
0	3.07	2.07	1.73	1.16	3.64	2.45	3.37	2.27
0.2	2.65	1.78	1.67	1.13	3.09	2.08	2.75	1.85
0.4	2.31	1.56	1.62	1.09	2.46	1.66	2.29	1.54
0.6	2.05	1.38	1.58	1.06	2.02	1.36	1.94	1.31
0.8	1.79	1.20	1.53	1.03	1.71	1.15	1.68	1.13
1.0*	1.48	1.00	1.48	1.00	1.48	1.00	1.48	1.00

*Case(i) temperature field

buckling strength is directly related to the amount of region that the panel is exposed to maximum temperature and bending stiffness of that region. Buckling strength of the CCCC panel-2 is higher than the panel-1 due to change in overall material properties associated with the lamination scheme. Table 16 depicts the magnification factor of first kind for a CCFC panel-2 exposed to different temperature fields. Data from Table 16 shows that, buckling temperature under case(i) temperature field has to be magnified by 2.07, 1.16, 2.45 and 2.27 to get the buckling temperature of panel-2 under case(ii), case(iii), case(iv) and case(v) respectively. Results shows that under CCFC boundary constraints, panel-2 with case(iv) temperature field has highest magnification factor but not so for CCCC boundary constraints. It is due to the fact that incase of case(iv) temperature field, the heat source is at the center of the panel-2 hence closer to the free edge therefore some of the stress set up due to thermal load will be relieved from the free edge.

To know the effect of aspect ratio, curvature ratio and thickness ratio on the buckling strength of the panel-2, parameter study has been carried out. Fig. 9(a)-(b) indicates the influence of temperature variation and the thickness ratio on the buckling strength of the panel-2 with CCCC and CCFC boundary constraints. It can be observed from Fig. 9 that like panel-1, panel-2 also follows the similar trend wherein its buckling strength decreases with the increase in thickness ratio and the same has been noted for all temperature fields. It can be seen from Figs. 5 and 9 that buckling strength of the panel-2 is higher than the panel-1, being un-symmetric in nature panel-2 is much stiffer than the panel-1 thus it offers lots of resistance against the membrane forces generated due to thermal load. Similar behavior is observed under all the temperature fields. Fig. 9 also reveals that irrespective of lamination scheme, free edge of the panel-2 influences the buckling strength of the panel-2. CCFC panel-2 has more buckling strength than the CCCC panel-2 under all temperature fields. Trend followed by the buckling temperature of CCFC panel-2 with the increase in thickness ratio is similar to CCCC panel-2 but with higher value. Like panel-1, even for panel-2 variation in the buckling temperature under different temperature fields is high at lower values of thickness ratio, but the variation tends to decrease with the increase in thickness ratio.

Effect of aspect ratio and temperature variation on panel-2 is shown in Fig. 10. It is further clear from Fig. 10 that buckling strength is significantly influenced by the aspect ratio. As observed for panel-1, even for panel-2 under case(ii), case(iii) and case(iv) temperature field buckling strength increases with the aspect ratio whereas it decreases under case(i) and case(v) temperature field. It is also observed from Fig. 10 that the variation in the buckling strength is

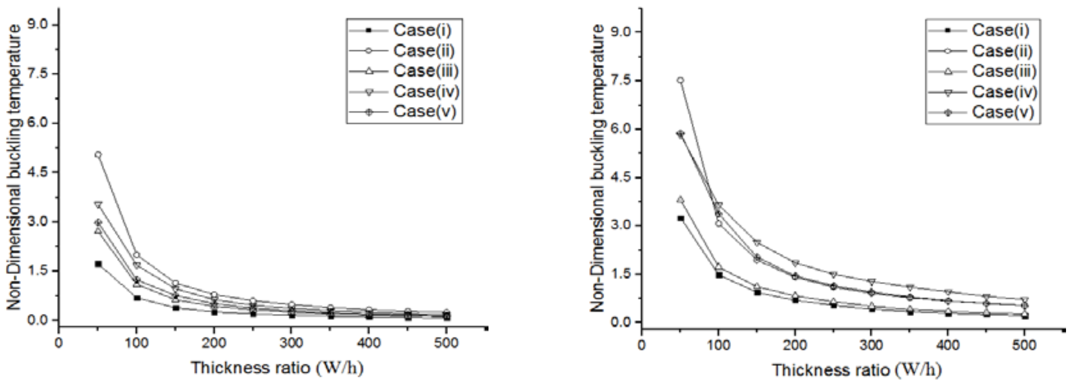

(a) CCCC (b) CCFC

Fig. 9 Influence of thickness ratio and temperature variation on buckling strength of cylindrical panel-2

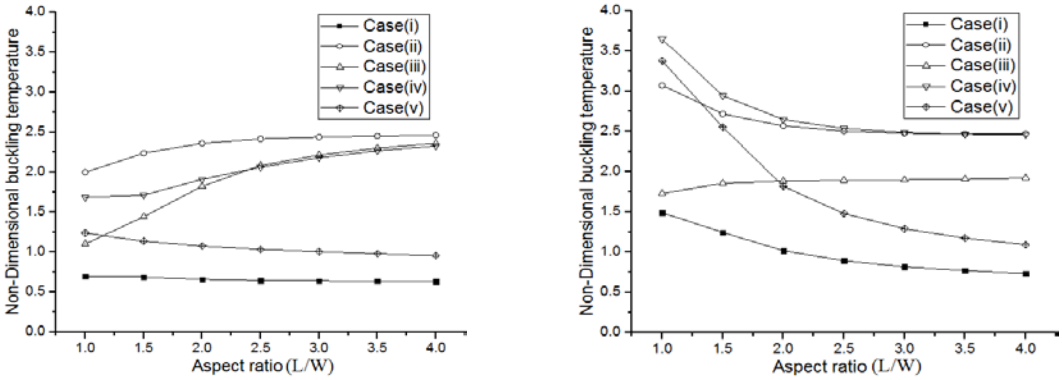

(a) CCCC (b) CCFC

Fig. 10 Influence of aspect ratio and temperature variation on buckling strength of cylindrical panel-2

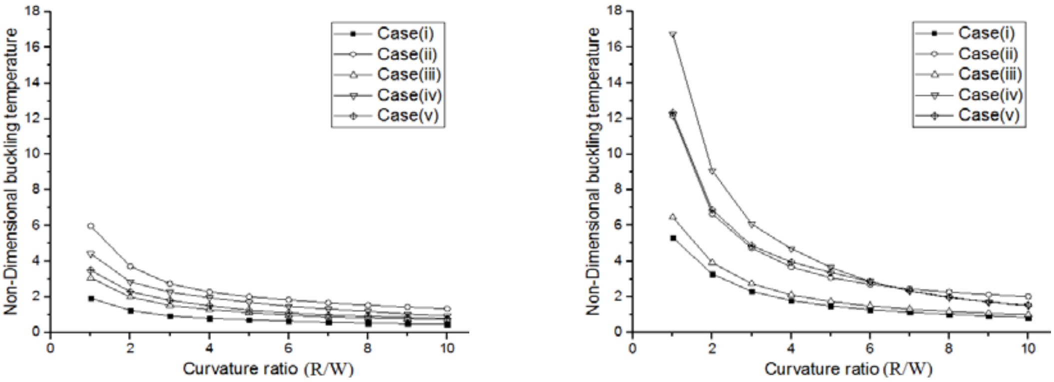

(a) CCCC (b) CCFC

Fig. 11 Influence of curvature ratio and temperature variation on buckling strength of cylindrical panel-2

much more significant for the panel-2 under CCFC boundary constraint compared to CCCC boundary constraint. Panel-2 under CCFC boundary constraints exposed to case(i), case(ii), case(iv) and case(v) temperature field has the similar behavior wherein buckling strength decreases with the aspect ratio. Furthermore, panel-2 under case(iii) temperature field, buckling temperature increases with the decrease in aspect ratio. Being buckling strength of the panel-2 is influenced by its curvature ratio, panel-2 is also analyzed for the variation in the curvature ratio. Influence of curvature ratio on the buckling temperature of the CCCC and CCFC panel-2 is depicted in Fig. 11(a)-(b) respectively. Where it can be observed that, buckling strength of the panel-2 decreases with the increase in curvature ratio and same behavior has been observed under CCCC and CCFC boundary constraints. Buckling strength of the panel-2 also depends on the moment of inertia of the panel-2 thus buckling strength behavior follows similar trend irrespective of temperature fields. As said in earlier discussions panel-2 has higher buckling strength than the panel-1 and same can be seen through Fig. 11. Due to free edge, panel-2 under CCFC boundary constraints has more buckling strength than CCCC boundary constraint.

Effect of thickness ratio on the buckling mode shape of CCCC panel-2 is shown in Table 17.

Compared to CCCC panel-1, change in buckling mode shape of the CCCC panel-2 is significant. It is due to subsequent change in thermal expansion with the ply orientation of un-symmetric panel-2 compared to symmetric panel-1 thus develops bending moment also along with the thermal stress. From Table 17 it is also observed that buckling mode shape of CCCC panel under a particular case of panel-1 and panel-2 is not same. Panel-1 with a thickness ratio of 100 under case(i) temperature field shows the modal indices of (1,3) whereas panel-2 with same thickness ratio observed to have modal indices of (2,2). Similar observation has been found for other temperature fields also. A cylindrical panel-2 by nature has high stiffness along the circumference

Table 17 Effect of thickness ratio on the buckling mode shape of CCCC panel-2

W/*h*	Case(i)	Case(ii)	Case(iii)	Case(iv)	Case(v)
100	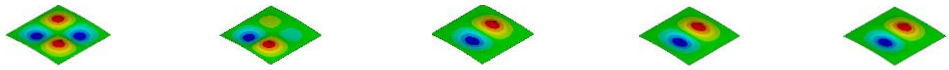				
200	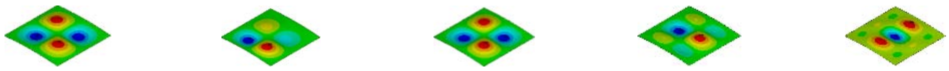				
300	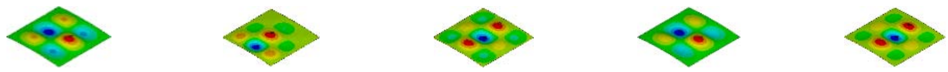				

*Note: Color gradients followed with dark-red and dark-blue indicate peak and trough buckling displacements, respectively

Table 18 Effect of thickness ratio on the buckling mode shape of CCFC panel-2

W/*h*	Case(i)	Case(ii)	Case(iii)	Case(iv)	Case(v)
100	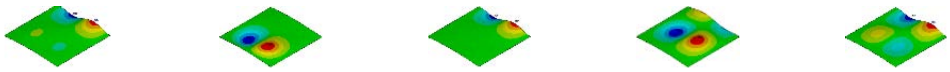				
200	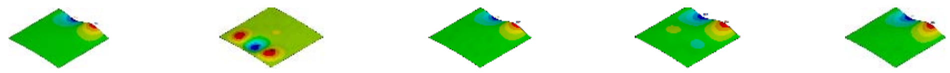				
300	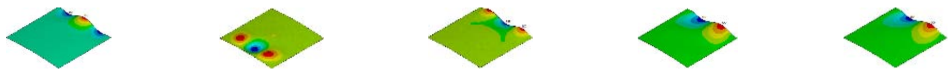				

*Note: Color gradients followed with dark-red and dark-blue indicate peak and trough buckling displacements, respectively

Table 19 Effect of curvature ratio on the buckling mode shape of CCCC panel-2

R/*W*	Case(i)	Case(ii)	Case(iii)	Case(iv)	Case(v)
1	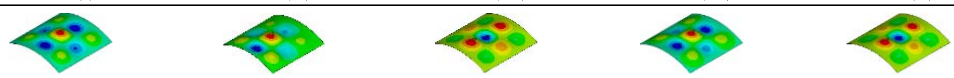				
5	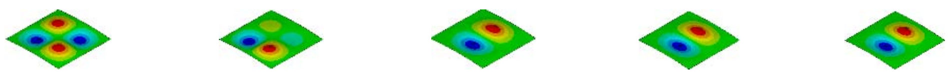				
10	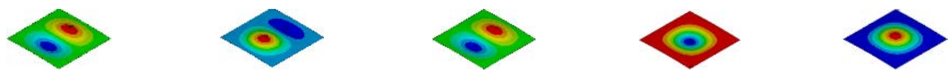				

*Note: Color gradients followed with dark-red and dark-blue indicate peak and trough buckling displacements, respectively

Table 20 Effect of curvature ratio on the buckling mode shape of CCFC panel-2

R/*W*	Case(i)	Case(ii)	Case(iii)	Case(iv)	Case(v)
1	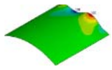	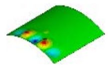	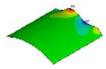	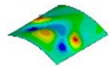	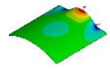
5	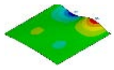	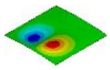	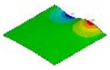	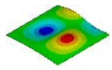	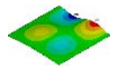
10	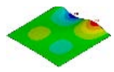	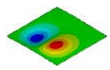	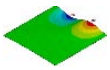	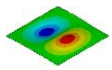	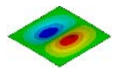

*Note: Color gradients followed with dark-red and dark-blue indicate peak and trough buckling displacements, respectively

and less stiffness along the length thus more number of buckling modes are observed along the length compared to the circumference as observed in panel-1 until there is some additional force/ moment acts on it, as seen in panel-2. It is also noted that, as the thickness ratio increases modal indices of the buckling modes are also increasing in both longitudinal and circumferential direction. This can be attributed to the change in structural stiffness with the thickness ratio. Table 18 shows the effect of thickness ratio and CCFC boundary constraints on the buckling mode shape of panel-2. Unlike panel-1, panel-2 was observed to have higher amplitude at the free edge under all temperature fields except case(ii) temperature field. Under case(ii) temperature field the heating source is located at the fixed edge, thus developing more membrane forces at that edge and making panel-2 to buckle.

Influence of curvature ratio and the temperature variation on the buckling mode shape of CCCC panel-2 is shown in Table 19. It can be seen from Table 19 that, CCCC panel-2 behaves similar to CCCC panel-1 when analyzed under different curvature ratio. Panel-2 at a lower curvature ratio is observed to have a higher number of modal indices in both the circumferential and longitudinal directions. Panel-2 at a curvature ratio of 1 has a similar pattern of modes under all temperature fields except for case(ii) temperature field due to un-symmetric associated with it. Table 20 shows the buckling modes of CCFC panel-2 at different curvature ratio. At lower values of curvature ratio, CCFC panel-2 under case(i)-, case(iii)-, case(v)- temperature fields are observed to have higher amplitudes at the free edge of the panel-2 due to less bending resistance offered by the free edge and the heating source of the panel-2. By comparing Table 9 and 20, it is observed that buckling modes of CCFC panel-1 has zero amplitude at the free edge, for most of the cases. This indicates that free edge behaves like a fixed edge as it is heated at buckling temperature. However, this is not the case for CCFC panel-2 mode shapes as seen in Table 20. This behavior of the panel-2 indicates that the variation in the stiffness due to lamination scheme used, plays a vital role in determining the buckling strength and its mode shape.

Effect of boundary constraints on the buckling temperature has been studied for panel-2. Under different types of non-uniform heating and results are given in Table 21. Like panel-1, panel-2 with CCCC boundary constraints observed to have minimum buckling strength compared to other structural boundary constraints. Similarly, panel-2 with SSSS boundary constraints was observed to have maximum buckling strength. Behavior of the panel-2 under different structural boundary constraints is similar to that of panel-1 under similar boundary constraints. Data from Table 21 shows that case(ii) temperature field has the maximum buckling temperature, whereas case(i) temperature field has the minimum under all boundary constraints.

Table 21 Effect of boundary constraints on non-dimensional buckling temperature of panel-2

Boundary constraints	Temperature variation fields				
	Case(i)	Case(ii)	Case(iii)	Case(iv)	Case(v)
CCCC	0.69	1.99	1.10	1.68	1.23
SSCC	1.54	7.50	2.79	3.14	2.96
SSSS	3.44	9.69	8.35	4.52	4.66
CCFC	1.48	3.07	1.72	3.64	3.37

Table 22 Effect of thermal load on free vibration frequency (Hz) of panel-2

Boundary constraints	Mode	At Ambnt. Temp.	Case(i)		Case(ii)		Case(iii)		Case(iv)		Case(v)	
			Critical buckling temperature, T_{cr} in %									
			50%	50%	50%	50%	50%	50%	50%	50%	50%	50%
CCCC	1	2233	1854	705	1852	704	1856	695	1736	705	1850	707
	2	2256	1964	937	1965	979	1944	962	1890	744	1924	1287
	3	2988	2189	1412	2242	1602	2149	1414	2157	1014	2162	1373
	4	3111	2211	1524	2361	1677	2262	1424	2336	1196	2387	1391
CCFC	1	2022	1568	517	1825	694	1573	522	1601	554	1500	521
	2	2110	1882	1151	2004	1508	1952	1552	1725	1072	1727	845
	3	2291	1950	1571	2052	1834	1975	1588	1961	1640	1914	1369
	4	2355	2116	1899	2131	2044	2109	1940	2038	1777	1952	1592

Free vibration analysis

To analyze the effect of lamination scheme on the behavioral trend of free vibration and its mode shape under thermal load, cylindrical panel-2 exposed to five different temperature variation fields is studied using pre-stressed modal analyzes. An investigation is carried out on cylindrical panel-2 with lamination scheme [0/90/0/90] and the analysis results are given in Table 22. As observed in panel-1 the natural frequency reduces with increase in temperature irrespective of the structural boundary constraints for panel-2 also. As stated earlier thermal stress and the bending moment produced due to thermal load and the un-symmetric ply orientation, affects the stiffness of the panel-2 thus reduces the frequency. Like panel-1, panel-2 also experiences the change in modal indices with increase in the thermal load. Table 23 shows the influence of thermal load on the free vibration mode shape of panel-2 under CCCC and CCFC boundary constraints. It is observed that modal indices of the fundamental vibration mode at ambient temperature is (2,1) which is shifted to (1,2) at near the critical buckling temperature. This shifting can be clearly observed for case(iii), case(iv) and case(v) temperature fields. Panel-2 under case(iii), case(iv) and case(v) temperature fields is observed to have more heat along the length thus it develops more stress along the length compared to circumferential direction which thus changes the geometrical stiffness accordingly and this results in change in modal indices. It is also observed that free vibration mode shape is influenced by the location of the heat source. Under case(i) temperature field vibration mode experiences the modal indices of (2,2) due to uniform distribution of heat along both circumferential and longitudinal directions. Table 23 also indicates the influence of free edge on

Table 23 Effect of thermal load on the free vibration mode shape of panel-2

	Mode	CCCC 1	CCCC 2	CCCC 3	CCCC 4	CCFC 1	CCFC 2	CCFC 3	CCFC 4
Temp. variation	At ambient temp.	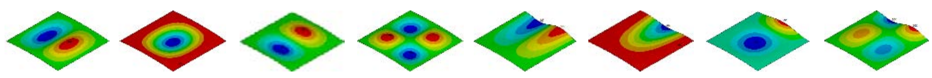							
Case(i)	50%T_{cr}	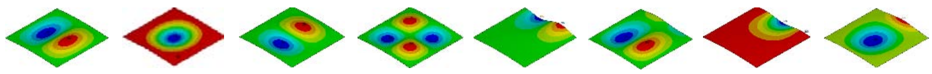							
	95%T_{cr}	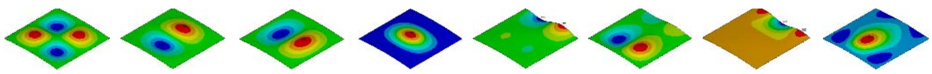							
Case(ii)	50%T_{cr}	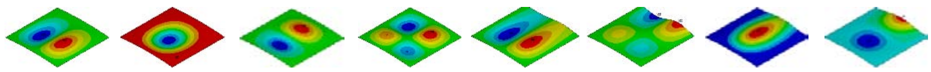							
	95%T_{cr}	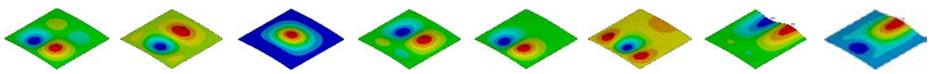							
Case(iii)	50%T_{cr}	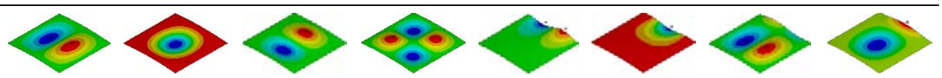							
	95%T_{cr}	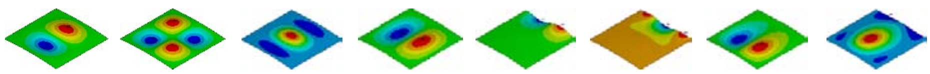							
Case(iv)	50%T_{cr}	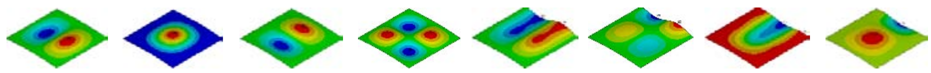							
	95%T_{cr}	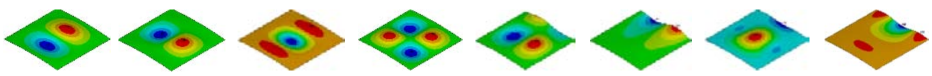							
Case(v)	50%T_{cr}	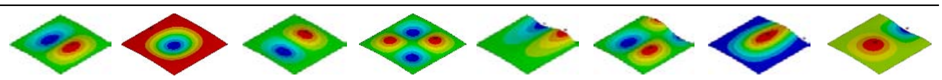							
	95%T_{cr}	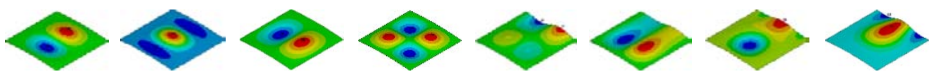							

the mode shape behavior. It can be noticed that like CCCC panel-2, CCFC panel-2 also experience the effect of thermal load on the free vibration mode shape and its modal indices. Thermal stress developed in the CCFC panel-2 is partly relieved from the free edge, thus change in modal shape and its modal indices is not so significant as observed for CCCC panel-2. It is seen that panel under case(i), case(iii) and case(v) temperature field shows similar behavior wherein the modes are observed to be at the free edge mainly due to stiffness and the heat source associated with the free edge. Whereas panel-2 under case(ii) and case(iv) temperature field behaves differently from the other temperature field due to location of heat source away from the free edge.

5. Conclusions

Present paper deals with the buckling and free vibration behavior of cylindrical panels exposed to different non-uniform temperature fields. Study has been carried out by using a numerical approach with the help of finite element tool. Material of the cylindrical panel throughout the analysis is assumed to have temperature independent properties. The outcomes of the present analysis indicate that the buckling and free vibration behavior of the cylindrical panels under thermal load is complex and significantly influenced by the lamination scheme, temperature field, fiber orientation, in-plane boundary constraints, elevated temperature and geometric parameters. Therefore, the following conclusion can be drawn:

- "Magnification factor of the first kind" established to predict the buckling strength of the panel under non-uniform temperature field knowing the buckling strength under uniform temperature field. Case(ii) temperature field was found to have highest magnification factor, 3.01 and 2.09 for a boundary constraints of CCCC and CCFC respectively.
- Geometrical parameters such as thickness ratio, curvature ratio and aspect ratio, play a dominant role in deciding the buckling strength of both panels analyzed. It is found that lowest thickness ratio (W/h = 75) and curvature ratio (R/W = 1) has the highest buckling strength.
- Present analysis also indicates that the buckling and free vibration behavior of the panel is significantly influenced of the lamination scheme of the panel. Un-symmetric lamination scheme gives better buckling strength compared to symmetric lamination scheme.
- Panels observed in the present analysis exposed to non-uniform temperature fields behaves totally different from the panels under uniform temperature field. This is due to additional thermal stress developed by the non-uniform temperature variations.
- Effect of non-uniform temperature fields variation on the buckling strength of the panel is more prominent on the stiffer panel.
- Shifting of nodal and anti-nodal lines and changing of modal indices with the rise in temperature has been observed through the present analysis.
- Further, first four free-vibration frequencies and their associated mode shapes are highly influenced by the temperature close to the buckling temperature considered in the present study.

References

Ahmadi, S.A. and Pourshahsavari, H. (2016), "Three-dimensional thermal buckling analysis of functionally graded cylindrical panels using differential quadrature method (DQM)", *J. Theor. Appl. Mech.*, **54**(1), 135-147.

Bhagat, V., Jeyaraj, P. and Murigendrappa, S.M. (2016a), "Buckling and free vibration characteristics of a uniformly heated isotropic cylindrical panel", *Procedia Enginering*, **144**, 474-481.

Bhagat, V., Jeyaraj, P. and Murigendrappa, S.M. (2016b), "Buckling and vibration behavior of a non-uniformly heated isotropic cylindrical panel", *Int. J. Struct. Eng. Mech.*, **57**(3), 543-567.

Chang, J.S. and Chiu, W.C. (1991), "Thermal buckling analysis of antisymmetric laminated cylindrical shell panels", *Int. J. Solid. Struct.*, **27**(10), 1295-1309.

Chen, L.W. and Chen, L.Y. (1987), "Thermal buckling of laminated cylindrical plates", *Compos. Struct.*, **8**(3), 189-205.

Eslami, M.R. and Javaheri, R. (1991), "Buckling of composite cylindrical shells under mechanical and thermal loads", *J. Therm. Stress.*, **22**(6), 527-545.

Ganapathi, M., Patel, B. and Pawargi, D. (2002), "Dynamic analysis of laminated cross-ply composite non-circular thick cylindrical shells using higher-order theory", *J. Solids Struct.*, **39**(24), 5945-5962.

Ganesan, N. and Pradeep, V. (2005), "Buckling and vibration of circular cylindrical shells containing hot liquid", *J. Sound Vib.*, **287**(4-5), 845-863.

Gupta, S.D. and Wang, I.C. (1973), "Thermal buckling of orthotropic cylindrical shells", *Fibre Sci. Technol.*,

6(1), 39-45.
Jeon, K.H.W., Byung H. and Lee, Y.S. (2010), "Free vibration characteristics of thermally loaded cylindrical shell", *Mater. Complex Behav.*, **3**, 139-148.
Jeyaraj, P. (2013), "Buckling and free vibration behavior of an isotropic plate under non-uniform thermal load", *Int. J. Struct. Stabil. Dyn.*, **12**(6), 1250071: 1-16.
Jooybar, N., Malekzadeh, P., Fiouz, A. and Vaghefi, M. (2016), "Thermal effect on free vibration of functionally graded truncated conical shell panels", *Thin-Wall. Struct.*, **103**, 45-61.
Kabir, H.R.H. (1998), "Free vibration response of shear deformable antisymmetric cross-ply cylindrical panels", *J. Sound Vib.*, **217**(4), 601-618.
Katariya, P.V. and Panda, S.K. (2016), "Thermal buckling and vibration analysis of laminated composite curved shell panel", *Aircraft Eng. Aerosp. Technol.*, **88**(1), 97-107.
Khdeir, A.A. (2012), "Thermoelastic response of cross-ply laminated shells based on a rigorous shell theory", *J. Therm. Stress.*, **35**(11), 1000-1017.
Ko, W.I. (2004), "Thermal buckling analysis of rectangular panels subjected to humped temperature profile heating", *Struct. Mech.*, **57**, 1-34.
Kurpa, L., Shmatko, T. and Timchenko, G. (2010), "Free vibration analysis of laminated shallow shells with complex shape using the R-functions method", *Compos. Struct.*, **93**(1), 225-233.
Lei, Z.X., Yu, J.L. and Liew, K.M. (2013), "Free vibration analysis of functionally graded carbon nanotube-reinforced composite cylindrical panels", *Int. J. Mater. Sci. Eng.*, **1**(1), 36-40.
Lei, Z., Zhang, L., Liew, K. and Yu, J. (2014), "Dynamic stability analysis of carbon nanotube-reinforced functionally graded cylindrical panels using the element free kp-ritz method", *Compos. Struct.*, **113**, 328-338.
Matsunaga, H. (2007), "Thermal buckling of cross-ply laminated composite shallow shells according to a global higher-order deformation theory", *Compos. Struct.*, **81**(2), 210-221.
Mochida, Y., Ilanko, S., Duke, M. and Narita, Y. (2012), "Free vibration analysis of doubly curved shallow shells using the Superposition-Galerkin method", *J. Sound Vib.*, **331**(6), 1413-1425.
Patel, B.P., Nath, Y. and Shukla, K.K. (2004), "Thermal buckling of laminated cross-ply oval cylindrical shell", *Compos. Struct.*, **65**(2), 217-229.
Patel, B.P., Nath, Y. and Shukla, K.K. (2007), "Thermo-elastic buckling characteristics of angle-ply laminated elliptical cylindrical shells", *Compos. Struct.*, **77**(1), 120-124.
Pradyumna, S. and Bandyopadhyay, J.N. (2010), "Free vibration and buckling of functionally graded shell panels in thermal environments", *Int. J. Struct. Stabil. Dyn.*, **10**(5), 1031-1053.
Rajanna, T., Banerjee, S., Desai, Y.M. and Prabhakara, D.L. (2016), "Vibration and buckling analyses of laminated panels with and without cutouts under compressive and tensile edge loads", *Steel Compos. Struct., Int. J.*, **21**(1), 37-55.
Shahab, S., Mirzaeifar, R. and Bahai H. (2009), "Coupled modification of natural frequencies and buckling loads of composite cylindrical panels", *Int. J. Mech. Sci.*, **51**(9-10), 708-717.
Shen, H.-S. (2012), "Thermal buckling and postbuckling behavior of functionally graded carbon nanotube-reinforced composite cylindrical shells", *Compos. Part B: Eng.*, **43**(3), 1030-1038.
Shen, H.S. and Li, Q.S. (2002), "Thermomechanical postbuckling of shear deformable laminated cylindrical shells with local geometric imperfections", *Int. J. Solids Struct.*, **39**(17), 4525-4542.
Thangaratnam, R., Palaninathan, R. and Ramachandran, J. (1990), "Thermal buckling of laminated composite shells", *Am. Inst. Aeronaut. Astronaut. J.*, **28**(5), 859-860.
Topal, U. (2012), "Frequency optimization for laminated composite plates using extended layerwise approach", *Steel Compos. Struct., Int. J.*,**12**(6), 541-548.
Topal, U. (2013), "Application of a new extended layerwise approach to thermal buckling load optimization of laminated composite plates", *Steel Compos. Struct., Int. J.*, **14**(3), 283-293.
Viswanathan, K.K., Lee, J.H., Aziz, Z.A. and Hossain, I. (2011), "Free vibration of symmetric angle-ply laminated cylindrical shells of variable thickness", *Acta Mech.*, **221**(3), 309-319.
Yas, M., Pourasghar, A., Kamarian, S. and Heshmati, M. (2013), "Three-dimensional free vibration analysis of functionally graded nanocomposite cylindrical panels reinforced by carbon nanotube", *Mater. Des.*, **49**,

583-590.
Zhang, L., Lei, Z., Liew, K. and Yu, J. (2014), "Static and dynamic of carbon nanotube reinforced functionally graded cylindrical panels", *Compos*. *Struct*., **111**, 205-212.
Zhao, X. and Liew, K.M. (2010), "A mesh-free method for analysis of the thermal and mechanical buckling of functionally graded cylindrical shell panels", *Computat*. *Mech*., **45**(4), 297-310.
Zhao, X., Ng, T.Y. and Liew, K. (2004), "Free vibration of two-side simply- supported laminated cylindrical panels via the mesh-free kp-ritz method", *Int*. *J*. *Mech*. *Sci*., **46**(1), 123-142.

CC